Mathematical Biosciences and Engineering

http://www.aimspress.com/journal/mbe

MBE, 22(9): 2458–2485.
DOI: 10.3934/mbe.2025090
Received: 13 April 2025
Revised: 29 June 2025
Accepted: 08 July 2025
Published: 24 July 2025

Research article

Targeting stem cells with oncolytic viruses: a mathematical modelling approach

Sana Jahedi[1,2,*], **Kamran Kaveh**[3] **and James Watmough**[4]

[1] Department of Mathematics and Statistics, Oakland University, Rochester, MI 48309, USA

[2] Department of Mathematics, University of Maryland, College Park, MD 20742, USA

[3] Therapy Modelling & Design Center, Department of Mathematics, University of Minnesota, Minneapolis, MN 55455, USA

[4] Department of Mathematics and Statistics, University of New Brunswick, Fredericton, NB, Canada

* **Correspondence:** Email: sjahedi.math@gmail.com.

Abstract: Intratumoural epigenetic heterogeneity, which affects the outcome of many cancer treatments, results from stem cell-differentiated cell hierarchy. Cancer stem cells, also known as tumour-initiating cells, are a pluripotent subpopulation of tumour cells capable of creating a tumour clone through self-renewal and differentiation. Oncolytic viral therapy is a category of cancer therapeutics with high specificity in targeting cancer cells while leaving normal cells unharmed. More recently, oncolytic viruses have been developed that target tumour initiating cells with some promising results. The question is what values for virus infectivity and stem cell specificity result in the best clinical outcome. To address this question, we model interactions between uninfected and infected cancer cells, within a stem cell-differentiated cell hierarchy, during oncolytic viral therapy. We calculate the basic reproduction number and use it to constrain the infectivity rates of initiating and differentiated cancer cells. Long-term tumour shrinkage is observable when this constraint is met; otherwise, treatment fails. Our results suggest that stem cell specificity of an oncolytic virus depends both on the average infectivity and mitotic rates of infected cells. There is a positive correlation between the average infectivity rate and stem cell specificity for nonmitotic infected cells: when average infectivity is high, an oncolytic virus with higher stem cell specificity leads to smaller tumours. In contrast, when average infectivity is low, the minimum tumour size is obtained when an oncolytic virus with higher potency targeting differentiated cells is used. For the perfect stem cell targeting regimen, we derive the condition that leads to the minimum tumour size.

Keywords: oncolytic virus; stem cell specificity; cancer stem cell; stem cell targeting; phenotypic heterogeneity; mathematical model; treatment strategies; virotherapy

1. Introduction

Tumour heterogeneity, which renders many conventional therapies ineffective, has been an important subject in cancer research for several decades [1–3]. Genomic heterogeneity inside tumours suggests random genetic alterations inside the genome of malignant cells induce resistance to radiation and chemotherapy. Phenotypic or epigenetic heterogeneities are as important as genomic heterogeneity. Phenotypic heterogeneity inside a tumour is both morphological and functional. One of the more important features of epigenetic heterogeneity in tumours is the fact that only a small subpopulation of cells, known as tumour initiating cells, or cancer stem cells, have the potential to create a tumour clone [4, 5]. These tumour initiating phenotypes have the potential to self-renew and differentiate via both symmetric and asymmetric proliferation events. This pluripotential capacity of tumour initiating cells leads to various heterogeneities inside a tumour. The phenotypic heterogeneity of tumours significantly impacts the effectiveness of treatment strategies. Tumour initiating cells have some common properties, such as long-lasting quiescence, high levels of multi-drug resistance expression, and high deoxyribonucleic acid (DNA) repair capability [6–8], which cause conventional therapies like chemotherapy [9] and radiotherapy [10] to fail in eradicating cancer stem cells. Hence, cancer stem cells are causative for tumour recurrence. It seems therapies not affected by the common properties of cancer initiating cells lead to more effective results.

Oncolytic viral therapy can be used as an alternative to chemo/radiation therapy to prevent drug resistance and the formation of new cancer cells [11]. Using tumour-specific promoters, oncolytic viruses can be engineered to target only cancer cells and not replicate in healthy normal cells. Therefore, oncolytic viral therapy has fewer side effects than conventional therapies. A category of viruses known as adenoviruses are widely used to engineer oncolytic viruses. It has been recently proposed that a successful oncolytic virus should be engineered to target cells with tumour initiating markers. By engineering a category of adenoviral vectors, Eriksson et al. [12] conducted a proof of concept study to show the effectiveness of oncolytic viruses against cancer stem cells. They showed that oncolytic viruses with E1A-CR2 capsid-modified adenoviruses could kill both quiescent and committed cancer stem cells [13].

Despite some promising results from in vitro and in vivo clinical trials [14–16], many questions remain unanswered about the overall promise of targeting tumour initiating cells using an oncolytic virus. Moreover, the treatment strategy and goal of such viral therapy could affect the design of the regimen. In principle, one can tune such treatment to target pre-cancerous small tumours or use it in combination with other anti-cancer therapies during a treatment course or just after/before remission to assure the leftover tumour initiating cells are eradicated [17, 18]. To do this, one needs a comprehensive yet simple model that incorporates a hierarchy of cells, including tumour initiating cells and differentiated cells in the presence of a cytotoxic oncolytic virus that targets different tumour cell types with different specificities and killing rates.

In the past two decades, some mathematical models have been introduced to describe the dynamics of each phenotype in a hierarchical structure of a tumour [19–21]. In addition, several mathematical models have been introduced to investigate oncolytic viral therapy [22–24]. However, there has not been any model that describes the oncolytic treatments in which cells from different phenotypes are targeted with different specificities. Here we build a mathematical model that describes interactions between populations of infected and uninfected cancer cells, where each of these populations is a

hierarchical structure of stem cell-differentiated cells, as illustrated in Figure 1.

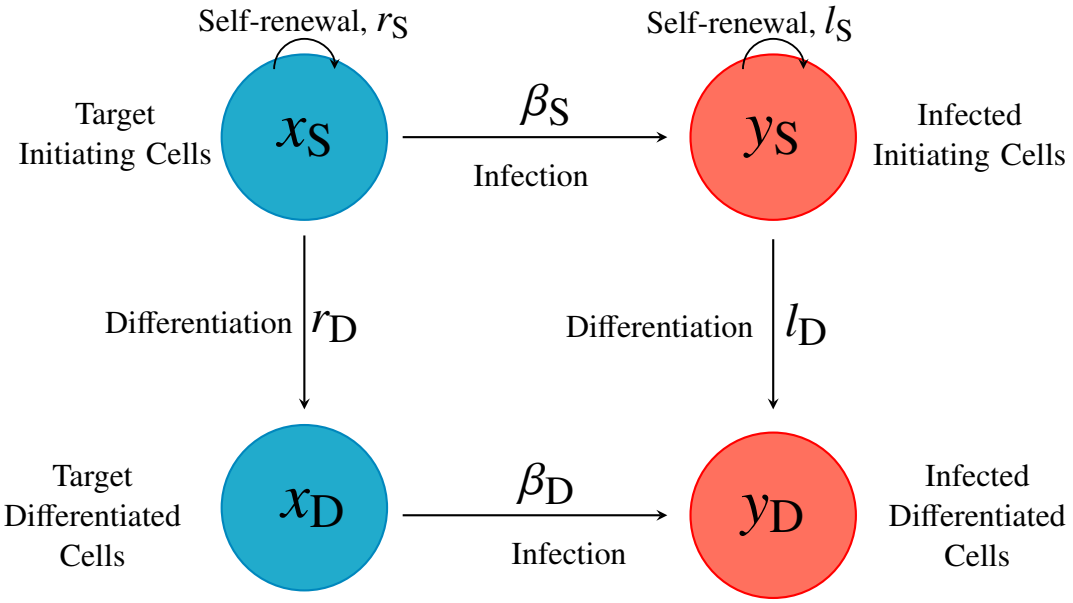

Figure 1. Schematic representation of vertical and horizontal transmission of infection within a tumour. x_S, x_D, y_S, and y_D represent target stem cells, target differentiated cells, infected stem cells, and infected differentiated cells, respectively.

The aim of our modelling effort is to address the following questions.

- Is tumour eradication possible by an oncolytic therapy in which both stem cells and their progenitors are targeted?
- Can we identify limits on infectivity of stem and differentiated cells that lead to a successful treatment?
- Which phenotype should preferentially be targeted to enhance the efficiency of therapy? In other words, does a higher specificity in targeting stem-like cancer cells increase the overall efficacy of the oncolytic viral therapy, or is a higher specificity in targeting differentiated tumour cells necessary?
- What is the optimal stem cell specificity to obtain the lowest tumour burden?
- What factors affect the optimal stem cell specificity?
- How do the infected cells' mitotic (self-renewal and differentiation) rates affect the therapeutic outcome?
- Does the stem cell fraction (the number of cancer stem cells/the total number of cancer cells) increase or decrease after oncolytic therapy?

The outcome of oncolytic viral therapy depends extensively on the extent to which infection invades the tumour [24]. An important measure widely used in epidemiology to identify transmissibility of

infection is the basic reproduction number [25]. Here, we use the basic reproduction number to find the constraint needed on the infectivity rates of stem and differentiated cells for the therapy to work. When this constraint is not satisfied, therapy fails.

In this work, we consider two different scenarios: mitotic and nonmitotic infected cells. We refer to an infected cell that cannot self-renew and differentiate as a nonmitotic infected cell. When infected cells are nonmitotic, virus transmission is only horizontal, meaning infection only is transmitted when an uninfected cell encounters free virus and becomes infected. We will show in this case tumours can only be partially infected. We refer to an infected cell that can self-renew and differentiate as a mitotic infected cell. When infected cells are mitotic, infection transmission occurs both horizontally and vertically. Vertical transmission occurs during self-renewal or differentiation. During self-renewal an infected stem cell divides into two infected daughter stem cells and during (symmetric) differentiation an infected stem cell gives birth to two infected differentiated cells. We derive a threshold at which infection fully invades the tumour. We show that optimal stem cell specificity is significantly impacted by the mitotic rates of infected cells.

2. Model: Oncolytic viruses targeting tumour initiating cells

Cancer stem cells are pluripotent because they can produce phenotypically different progenies from the original mother stem cell; this can be achieved through symmetric and asymmetric divisions where the daughter cell is either a stem cell or an early progenitor [26]. Progenitor or partially differentiated cells which divide through a chain of proliferation events give rise to a larger population of fully differentiated cells [27]. In this work, we only consider symmetric cell divisions. During the self-renewal process, a stem cell gives rise to two identical daughter stem cells, as illustrated in Figure 2(a). During the symmetric differentiation process, a stem cell divides into two differentiated cells, see Figure 2(b) for a schematic representation.

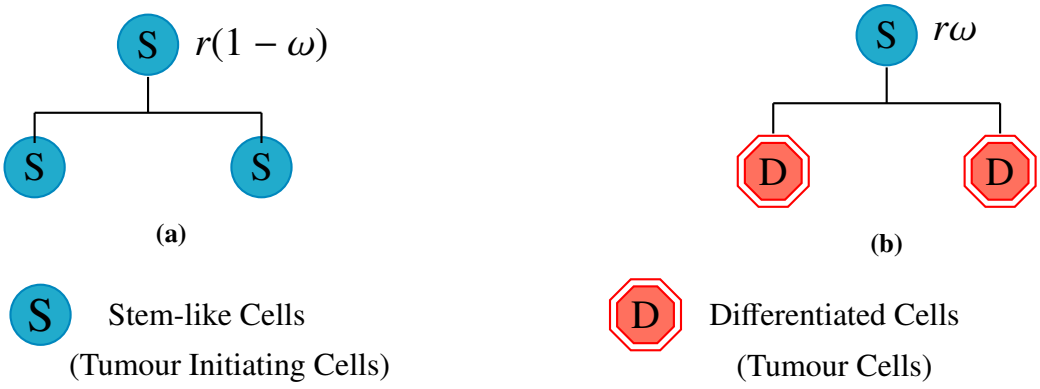

Figure 2. A simplified hierarchy of symmetric divisions of tumour initiating cells. This figure is a schematic representation of symmetric cell divisions of stem cells. Here we assume the stem cell division rate is r and $(1-\omega)$ is the self-renewal probability. Plot (a) represents self-renewal, meaning a stem cell divides into two daughter stem cells with rate $r_S = r(1-\omega)$. Plot (b) shows the differentiation process in which a stem cell divides symmetrically into two differentiated cells with rate $r\omega$.

For simplicity, we use a simplified two-compartment model where stem cells are collected in one compartment and partially or fully differentiated cells are in another. The following system of equations gives this simplified model.

$$\frac{\mathrm{d}x_\mathrm{S}}{\mathrm{d}t} = r(1-\omega)x_\mathrm{S}(1-b_\mathrm{S}x_\mathrm{S}) - \bar{d}_\mathrm{S}x_\mathrm{S} - r\omega(1-b_\mathrm{D}x_\mathrm{D})x_\mathrm{S}, \tag{2.1a}$$

$$\frac{\mathrm{d}x_\mathrm{D}}{\mathrm{d}t} = \alpha r\omega(1-b_\mathrm{D}x_\mathrm{D})x_\mathrm{S} - d_\mathrm{D}x_\mathrm{D}, \tag{2.1b}$$

where x_S and x_D are the population densities of stem cells and differentiated cells, respectively. The stem cell division rate is denoted by r and ω is the differentiation probability. We assume that stem cells self-renew with the rate $r(1-\omega)$; in the rest of this paper we denote the self-renewal rate of stem cells with r_S, that is $r_\mathrm{S} = r(1-\omega)$. We further assume that stem cell self-renewal is regulated by cell density. In particular, self-renewal declines with increasing stem cell density and vanishes when the density reaches $1/b_\mathrm{S}$. Accordingly, b_S quantifies the strength of this density-dependent feedback, representing the per-capita rate at which crowding inhibits stem cell self-renewal. The apoptosis rate of stem cells is denoted by $\bar{d}_\mathrm{S}$. The rate of differentiation is $r\omega$ and $\alpha \geq 2$ is a variable denoting the final number of fully differentiated cells that are reproduced by a stem cell that has undergone differentiation. Herein for simplicity we let $r_\mathrm{D} = \alpha r\omega$.

In Eq (2.1b) the apoptosis rate of fully differentiated cells is denoted by d_D. To model tumour nutrient limitations, we assume that stem cell differentiation is density-dependent, decreasing as the density of differentiated cells increases. Differentiation is completely halted when the density of differentiated cells reaches $1/b_\mathrm{D}$. The parameter b_D characterizes the strength of this inhibitory effect: b_D represents the rate at which differentiated cells suppress stem cell differentiation due to crowding. Different critical densities are used for stem and differentiated cells because stem cells are assumed to be confined to stem cell niches, which restrict their maximum density. In contrast, differentiated cells are not subject to the same spatial constraints, and their density can be much higher in practice [28]; hence, $b_\mathrm{D} \ll b_\mathrm{S}$. Therefore, we can assume $b_\mathrm{D} = 0$. Under this assumption the system of Eq (2.1) simplifies to

$$\frac{\mathrm{d}x_\mathrm{S}}{\mathrm{d}t} = r_\mathrm{S}x_\mathrm{S}(1-b_\mathrm{S}x_\mathrm{S}) - \bar{d}_\mathrm{S}x_\mathrm{S} - r\omega x_\mathrm{S},$$

$$\frac{\mathrm{d}x_\mathrm{D}}{\mathrm{d}t} = r_\mathrm{D}x_\mathrm{S} - d_\mathrm{D}x_\mathrm{D}.$$

As of now for simplicity we abbreviate $\bar{d}_\mathrm{S} + r\omega$ by d_S. Note that when $b_\mathrm{D} = 0$, d_S denotes the removal rate of cancer stem cells. Under the new notation the above model simplifies to

$$\frac{\mathrm{d}x_\mathrm{S}}{\mathrm{d}t} = r_\mathrm{S}x_\mathrm{S}(1-b_\mathrm{S}x_\mathrm{S}) - d_\mathrm{S}x_\mathrm{S}, \tag{2.2a}$$

$$\frac{\mathrm{d}x_\mathrm{D}}{\mathrm{d}t} = r_\mathrm{D}x_\mathrm{S} - d_\mathrm{D}x_\mathrm{D}. \tag{2.2b}$$

One example of a well-defined stem cell population is the colorectal stem cell population. They reside on the base of cylindrical-shaped structures called crypts [29–31]. When stem cells divide into stem cells, the offspring remain in the crypt base. Upon differentiation, the differentiated daughter cells

move up across the crypt. Thus, the population keeps a hierarchy, and the stem cell population in the niche remains distinct from the differentiated progenitors [32, 33]. Model (2.2) encapsulates the main features of a hierarchical structure of stem cell-differentiated cell proliferation inside a tumour. We use the above simple stem cell-differentiated cell hierarchy to model the cancer cell dynamics during oncolytic therapy.

The primary function of oncolytic viruses is to infect and lyse tumour cells. However, an oncolytic viral therapy in which both stem and differentiated cells are targeted involves many complexities. For example, tumour initiating cells and differentiated cells might become infected at different rates [34]. The number of copies that a free virus makes in a host infected cell may vary depending on the phenotype of the infected cell [35]. Here, our goal is to introduce a very simple model that describes the evolution of both cancer stem cells and differentiated cells during an oncolytic viral therapy that targets both stem cells and differentiated cells. Therefore, we make some simplifying assumptions that ignore some of these complexities.

We begin by writing a four-compartment model which includes target stem cells, x_S, target differentiated cells, x_D, infected stem cells, y_S, and infected differentiated cells, y_D, see Figure 1. In the absence of treatment, stem cells and differentiated cells follow the dynamics discussed in Model (2.2). A stem cell encounters an infected cell and becomes infected at rate β_S. A differentiated cell encounters an infected cell and becomes infected at rate β_D. The self-renewal rate of infected stem cells is denoted by l_S and the differentiation rate of infected stem cells is denoted by l_D, see Figure 1. The removal rate of infected stem cells is denoted by a_S. The apoptosis rate of infected differentiated cells is denoted by a_D. A summary of all the parameters with their corresponding biological interpretations is provided in Table 1.

The above dynamics are given by the following system of equations:

$$\frac{dx_S}{dt} = r_S x_S(1 - b_S(x_S + y_S)) - d_S x_S - \beta_S x_S(y_S + y_D), \tag{2.3a}$$

$$\frac{dx_D}{dt} = r_D x_S - d_D x_D - \beta_D x_D(y_S + y_D), \tag{2.3b}$$

$$\frac{dy_S}{dt} = l_S y_S(1 - b_S(x_S + y_S)) - a_S y_S + \beta_S x_S(y_S + y_D), \tag{2.3c}$$

$$\frac{dy_D}{dt} = l_D y_S - a_D y_D + \beta_D x_D(y_S + y_D). \tag{2.3d}$$

The following are the assumptions under which we will study the dynamics of Model (2.3).

A1: The virus turnover is much faster than the turnover of infected cells, so the virus is in a quasi-steady state; that is why there is no equation for the dynamics of free virus.

A2: The burst size of the free virus is the same for both cancer stem cells and cancer differentiated cells.

A3: The vertical infection transmission is perfect in that an infected cell does not produce any uninfected daughter cells through self-renewal or differentiation.

A4: Per capita growth rates of target cancer cells are greater than their removal rates, $r_S > d_S$ and $r_D > d_D$.

A5: The virus is virulent; infection reduces cell growth and elevates apoptosis. Hence, $l_S < r_S$ and $l_D < r_D$, $a_S > d_S$ and $a_D > d_D$.

Table 1. Summary of parameters.

Symbol	Biological interpretation	Units
b_S	the rate at which stem cells inhibit stem cell self-renewal due to crowding	$[\text{cell}]^{-1}$
b_D	the rate at which differentiated cells inhibit stem cell differentiation due to crowding	$[\text{cell}]^{-1}$
β_S	infectivity rate per stem cell	$[\text{day}]^{-1}[\text{cell}]^{-1}$
β_D	infectivity rate per differentiated cell	$[\text{day}]^{-1}[\text{cell}]^{-1}$
r_S	self-renewal rate for target stem cells	$[\text{day}]^{-1}$
l_S	self-renewal rate for infected stem cells	$[\text{day}]^{-1}$
r_D	α times the rate of symmetric differentiation for target stem cells	$[\text{day}]^{-1}$
l_D	α times the rate of symmetric differentiation for infected stem cells	$[\text{day}]^{-1}$
d_D	apoptosis rate of target differentiated cells	$[\text{day}]^{-1}$
a_D	apoptosis rate of infected differentiated cells	$[\text{day}]^{-1}$
d_S	removal rate (i.e. the sum of the apoptosis rate and differentiation rate) of target stem cells	$[\text{day}]^{-1}$
a_S	removal rate (i.e. the sum of the apoptosis rate and differentiation rate) of infected stem cells	$[\text{day}]^{-1}$
r	stem cell division rate	$[\text{day}]^{-1}$
ω	differentiation probability	unitless
α	final number of fully differentiated cells	unitless

In addition to the above assumptions, in our numerical simulations, illustrated in Figures 3–5, we rescale Model (2.3) by choosing $b_S = 1$; under this rescaling, the state variables x_S, x_D, y_S, and y_D become dimensionless. To reflect this rescaling, we define the *relative tumour size* as $b_S(x_S + x_D + y_S + y_D)$, which simplifies to the sum $x_S + x_D + y_S + y_D$ when $b_S = 1$. Note that this rescaling also affects the interpretation of the infectivity parameters β_S and β_D, which must now be divided by b_S. Assuming the unit of time is days, the parameters β_S/b_S and β_D/b_S then have units of day^{-1}.

The main question of this paper is how hierarchical phenotypic variability affects the mechanism of tumour infection by the virus. The engineered virus used in the experiments targets some common tumour suppressor gene promoters. To engineer viruses with the capability of targeting stem cells, an additional stem cell marker is added to increase the specificity of the virus while the infectivity to the non-stem-like tumour cells is not changed. Specificity and infectivity of the virus encountering tumour initiating (tumour differentiated) cells are incorporated in β_S (β_D). In this work, we will focus on how changes in β_S and β_D affect the outcome of the therapy.

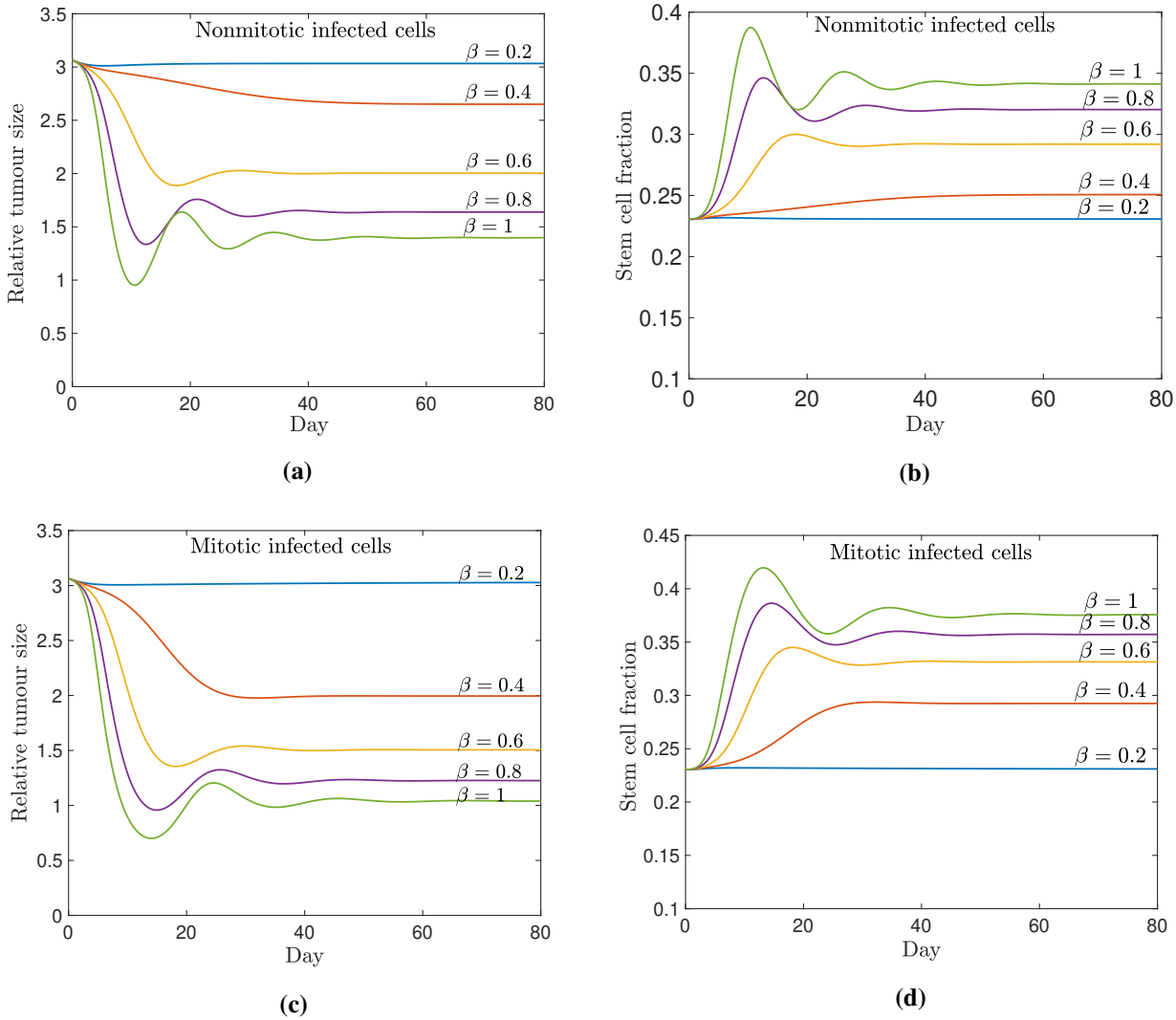

Figure 3. Effect of average infectivity on tumour size and stem cell fraction under random targeting. Panels (a) and (c) illustrate that increasing average infectivity reduces tumour size, while panels (b) and (d) show that the stem cell fraction increases with infectivity. As mentioned in Section 2, relative tumour size is a dimensionless quantity, representing the total tumour burden relative to the maximum density of cancer stem cells, see the text for details. In panels (a) and (b), infected cells are nonmitotic ($l_S = l_D = 0$); in panels (c) and (d), infected cells are mitotic ($l_S = 0.25$, $l_D = 0.5$). This simulation corresponds to Model (2.3) with $\beta_S = \beta_D = \beta$, where $\beta \in \{0.2, 0.4, \ldots, 1.0\}$. Other model parameters are: $r_S = 1$, $r_D = 2$, $d_S = 0.3$, $d_D = 0.6$, $a_S = d_S + 0.01$, $a_D = d_D + 0.01$, and $b_S = 1$. Initial conditions are: $x_S(0) = 0.012$, $x_D(0) = 0.012$, $y_S(0) = 0.012x_S(0)$, and $y_D(0) = 0.012x_D(0)$.

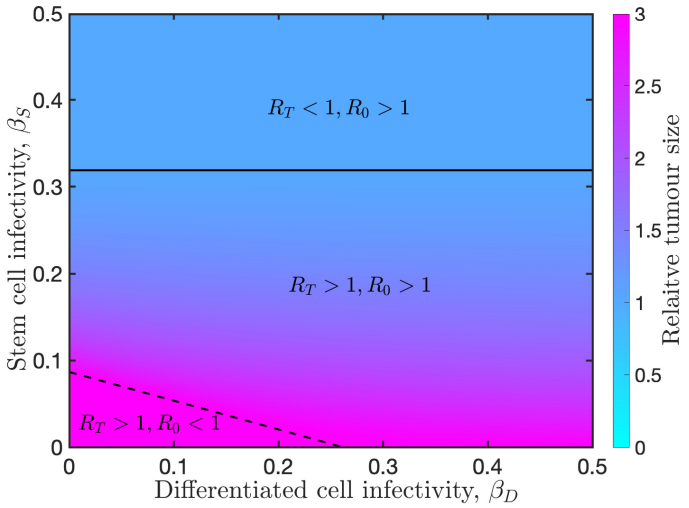

Figure 4. Heat map of tumour burden post therapy as a function of β_S, β_D. The tumour steady state is plotted as a function of β_D and β_S. This is superimposed with the regions in the (β_S, β_D) plane that are separated by lines $R_0 = 1$ and $R_T = 1$ where R_0 is the basic reproduction number of the virus (Eq (3.5)) and R_T is the reproduction number of uninfected cancer cells (Eq (3.9)). The dashed line represents $R_0 = 1$. The maximum tumour size under treatment occurs when $R_0 < 1$. The solid line represents $R_T = 1$. Tumour size reduces as β_S increases, and it becomes minimum when $R_T = 1$. In the area labelled as $R_T < 1$, changes in β_S or β_D do not affect the tumour size. This simulation corresponds to a positive net growth rate (self-renewal rate – removal rate) of infected cancer stem cells. When the net growth rate of infected cancer stem cells tends to zero, the line $R_T = 1$ tends to infinity. (Model parameters are: $r_S = 1, r_D = 2r_S, d_S = 0.3, d_D = 0.6, l_S = 0.5, l_D = 2l_S, a_S = d_S + 0.01, a_D = d_D + 0.01, b_S = 1, b_D = 0.$)

3. Results

3.1. Steady states

The tumour size post-therapy is a measure of the success of any cancer treatment. Hence, it is important to identify the steady states of the model and their stability to understand the long-term outcomes of the treatment. We use a vector $E = (x_S, x_D, y_S, y_D)$ to refer to steady states. For any given set of parameters, Model (2.3) has at most four steady states, each corresponding to a different treatment outcome.

- The tumour eradication steady state, $E_0 = (0, 0, 0, 0)$.
- The treatment failure steady state, $E_T = (x_{TS}, x_{TD}, 0, 0)$.

$$x_{TS} = \frac{r_S - d_S}{b_S r_S}, \tag{3.1a}$$

$$x_{TD} = \frac{r_D}{d_D} x_{TS}. \tag{3.1b}$$

- The 100% infection prevalence steady state, $E_{\mathrm{I}} = (0, 0, y_{\mathrm{IS}}, y_{\mathrm{ID}})$.

$$y_{\mathrm{IS}} = \frac{l_{\mathrm{S}} - a_{\mathrm{S}}}{l_{\mathrm{S}} b_{\mathrm{S}}}, \tag{3.2a}$$

$$y_{\mathrm{ID}} = \frac{l_{\mathrm{D}}}{a_{\mathrm{D}}} y_{\mathrm{IS}}. \tag{3.2b}$$

- The partially infected steady state, $E_{\mathrm{p}} = (x_{\mathrm{S}}^*, x_{\mathrm{D}}^*, y_{\mathrm{S}}^*, y_{\mathrm{D}}^*)$. For the closed form of the partially infected steady state see Section 5.1.

Theorem 1 states the constraints on β_{S} and β_{D} values, under which the above steady states exist.

Theorem 1.

(I): The steady state E_T always exists under assumption (A4) .

(II): The steady state E_{I} exists if and only if infected cells are mitotic and the self-renewal rate of infected cancer stem cells is greater than their removal rate; equivalently, $l_{\mathrm{S}} \neq 0$, $l_{\mathrm{D}} \neq 0$, and $l_{\mathrm{S}} > a_{\mathrm{S}}$.

(III): When $a_{\mathrm{S}} < l_{\mathrm{S}}$ and $1 < \dfrac{r_{\mathrm{D}}}{a_{\mathrm{D}} + l_{\mathrm{D}}} < \dfrac{r_{\mathrm{S}}}{l_{\mathrm{S}}}$, there exists a unique interior steady state if

$$\left(\frac{a_{\mathrm{S}} r_{\mathrm{S}} - d_{\mathrm{S}} l_{\mathrm{S}}}{a_{\mathrm{D}} + l_{\mathrm{D}}}\right) \frac{b_{\mathrm{S}} d_{\mathrm{D}} a_{\mathrm{D}} r_{\mathrm{S}} - \beta_{\mathrm{D}} r_{\mathrm{D}} (r_{\mathrm{S}} - d_{\mathrm{S}})}{r_{\mathrm{S}} d_{\mathrm{D}} (r_{\mathrm{S}} - d_{\mathrm{S}})} < \beta_{\mathrm{S}} < \frac{b_{\mathrm{S}} a_{\mathrm{D}} (r_{\mathrm{S}} a_{\mathrm{S}} - l_{\mathrm{S}} d_{\mathrm{S}})}{(l_{\mathrm{S}} - a_{\mathrm{S}})(a_{\mathrm{D}} + l_{\mathrm{D}})}. \tag{3.3}$$

(IV): When $l_{\mathrm{S}} = l_{\mathrm{D}} = 0$, there exists a unique interior steady state if

$$\beta_{\mathrm{S}} > \frac{a_{\mathrm{S}} (a_{\mathrm{D}} d_{\mathrm{D}} b_{\mathrm{S}} r_{\mathrm{S}} - \beta_{\mathrm{D}} r_{\mathrm{D}} (r_{\mathrm{S}} - d_{\mathrm{S}}))}{a_{\mathrm{D}} d_{\mathrm{D}} (r_{\mathrm{S}} - d_{\mathrm{S}})}. \tag{3.4}$$

See Section 5.2 for the proof of the above theorem.

Earlier research on oncolytic viral therapy that does not consider phenotypic heterogeneity suggests that increasing the transmission rate enhances therapeutic effectiveness by reducing tumour size [24, 36]. Numerical simulations of Model (2.3), in which cancer cells are randomly targeted, i.e., $\beta_{\mathrm{S}} = \beta_{\mathrm{D}} = \beta$, support these earlier findings; see Figure 3. Our simulations further show that for very small values of β, tumour size remains largely unaffected. However, increasing β leads to a notable reduction in tumour size following treatment, both in the case of mitotic and nonmitotic infected cells. Despite this reduction, the tumour burden does not vanish completely, even for large values of β. Additionally, for the same value of β, treatment is more effective (leads to greater tumour reduction) when infected cells are mitotic; see panels (a) and (c) in Figure 3.

Our numerical results also suggest that increasing the average infectivity raises the stem cell fraction, indicating that the therapy is more effective at eliminating differentiated cancer cells. This trend is illustrated in panels (b) and (d) in Figure 3.

In Section 3.2, we show that in the case of mitotic infected cells, increasing the average infectivity initially reduces the tumour size which is consistent with the results described above. However, this effect is not unbounded: there exists a threshold for the transmission rate of infection to stem cells beyond which further increases in infectivity no longer reduce tumour size. Moreover, our results demonstrate that virus specificity, preferentially targeting one phenotype over another, plays a crucial role in treatment outcomes. In particular, effectively targeting cancer stem cells is essential for achieving maximal tumour reduction.

3.2. The reproduction number of cancer cells identifies treatment outcomes

The eigenvalues of the Jacobian of Model (2.3) at E_0 are $r_S - d_S$, $l_S - a_S$, $-d_D$, and $-a_D$. By assumption (A4), $r_S - d_S > 0$ and the Jacobian of Model (2.3) at E_0 always has at least one positive eigenvalue. Therefore, under assumption (A4) E_0 is unstable: our model suggests that even an oncolytic viral therapy in which cancer cells from different phenotypes are targeted with different specificities cannot eradicate the tumour. However, our simulations suggest that the long-term tumour shrinkage after therapy is observable when the infection spreads through the tumour cells, and the tumour becomes partially or fully infected; when the basic reproduction number is larger than one infection can invade the tumour. The basic reproduction number, R_0, is defined as the expected number of newly infected cells produced by a typical infected cell when the tumour is at the steady state E_T. The following lemma gives a closed form for R_0.

Lemma 1. The basic reproduction number R_0 corresponding to Model (2.3) is given by

$$R_0 = \frac{\mathrm{tr}(\mathscr{N}_I)}{2} + \sqrt{\left(\frac{\mathrm{tr}(\mathscr{N}_I)}{2}\right)^2 - \det(\mathscr{N}_I)}\,, \tag{3.5}$$

where

$$\mathscr{N}_I = \begin{pmatrix} \dfrac{l_S d_S}{a_S r_S} + \dfrac{x_{TS}\beta_S}{a_S} & \dfrac{x_{TS}\beta_S}{a_D} \\ \dfrac{l_D}{a_S} + \dfrac{x_{TD}\beta_D}{a_S} & \dfrac{x_{TD}\beta_D}{a_D} \end{pmatrix}. \tag{3.6}$$

In the above lemma, N_I is the next generation matrix of infected cells for Model (2.3). To calculate the next generation matrix, we use the method given by van den Driessche and Watmough in 2002 [25]. See Section 5.3 for the algebraic calculations of $\mathscr{N}_I$ and the proof of Lemma 1.

In the special case when the virus transmission is only horizontal, so that $l_S = l_D = 0$, the basic reproduction number is given by

$$R_{0,\mathrm{nonmitotic}} = \frac{1}{b_S}\left(\frac{\beta_S}{a_S} + \frac{\beta_D}{a_D}\frac{r_D}{d_D}\right)\left(1 - \frac{d_S}{r_S}\right) = \frac{x_{TS}\beta_S}{a_S} + \frac{x_{TD}\beta_D}{a_D}. \tag{3.7}$$

The above formula shows the basic reproduction number is proportional to the number of new exposures and new infections as expected. To interpret the expression, note that the lifetime of an infected cancer stem cell is $1/a_S$ with each cancer stem cell producing $\beta_S x_{TS}$ infected tumour stem cells in its life time and the lifetime of an infected differentiated cell is $1/a_D$ with each infected differentiated cell producing $\beta_D x_{TD}$ infected differentiated cells in its lifetime, so each infected cell in its lifetime produces R_0 infected individuals.

As we mentioned above, we are interested in the case where $R_0 > 1$. The following Theorem identifies the constraint on the parameter space under which $R_0 > 1$.

Theorem 2. $R_0 > 1$ if and only if

$$\beta_S > \left(\frac{b_S a_D}{r_S - d_S} - \beta_D \frac{r_D}{r_S d_D}\right)\frac{r_S a_S - l_S d_S}{l_D + a_D}. \tag{3.8}$$

See Section 5.4 for the proof of this theorem.

Corollary 1. Note that the lower bound for β_S in Eq (3.8), inequality (3.3), and inequality (3.4) is the same. Hence, by Theorem 2, the lower bound condition on β_S in part (III) and part (IV) of Theorem 1 can be replaced by the condition $R_0 > 1$.

It is essential to understand that once most of the tumour cells become infected and uninfected cancer cells are rare, the population of uninfected cancer cells may still regrow and partially or fully invade the tumour. To determine the conditions under which this occurs, we need to calculate the reproduction number of uninfected cancer cells. The reproduction number of an uninfected cancer cell is the number of new uninfected cancer cells that an uninfected cancer cell produces in its lifetime when Model (2.3) is in E_I steady state. Let R_T denote the reproduction number of uninfected cancer cells:

$$R_T = \left(\frac{r_S}{d_S + \beta_S(y_{IS} + y_{ID})}\right)\frac{a_S}{l_S}. \tag{3.9}$$

See Section 5.5 for the details of the algebraic calculations of R_T.

Note that R_T is only defined when infected cells are mitotic ($l_S > 0$). As stated previously, the steady state E_I only exists if infected cells are mitotic ($l_S, l_D > 0$) and the net growth rate of infected cancer stem cells is positive in the absence of horizontal infection ($l_S > a_S$).

We are interested in the case where all the tumour cells are infected, and uninfected cells can no longer outgrow the infected ones; this happens when $R_T < 1$. By Eq (3.9) R_T is smaller than one if and only if

$$\beta_S > \frac{b_S a_D(r_S a_S - l_S d_S)}{(l_S - a_S)(a_D + l_D)}. \tag{3.10}$$

Corollary 2. Note that $R_T > 1$ if and only if the right-hand inequality in (3.3) holds. Hence, the upper bound condition on β_S in part (III) of Theorem 1 could be replaced by the condition $R_T > 1$.

Treatment outcomes are as follows.

(I) **Treatment failure:** When $R_0 < 1$, E_T (infection free equilibrium) is locally asymptotically stable [25]. Our numerical simulations suggest that when $R_0 < 1$, E_T is globally stable, in the sense that it attracts every solution that starts from a positive initial condition. Hence, when $R_0 < 1$ our simulations suggest that infection cannot invade the tumour and treatment fails. Figure 4 is a heat map of tumour size post-therapy as a function of the two transmission rates, β_S and β_D. As this figure illustrates, the largest tumour size post-therapy occurs when $R_0 < 1$. The figure suggests that if the rate at which stem cells become infected, β_S, and the rate at which fully differentiated cells become infected, β_D, belong to the area labelled by $R_0 < 1$, treatment fails. In such a case, either there will be no tumour shrinkage, or there may be a small tumour shrinkage at the beginning of the therapy. However, the tumour eventually follows the same dynamics as in the absence of the therapy. If this scenario occurs, the steady-state tumour size post-therapy will be the same as the tumour size in the steady state E_T, $x_{TS} + x_{TD} = (r_S - d_S)(d_D + r_D)/(r_S b_S d_D)$.

(II) **Partial success:** When $R_0 > 1$ and either $l_S < a_S$ or $R_T > 1$, infection partially invades the tumour, some tumour cells become infected, and the tumour size decreases considerably. By Theorem 1, Corollary 1, and Corollary 2, there exists a unique interior equilibrium: in the mitotic case when both R_T and R_0 are greater than one (see Theorem 1 for the remaining constraints on the parameter space), and in the nonmitotic case when $R_0 > 1$. Our numerical simulations suggest that

this unique interior equilibrium is globally stable: eventually, the tumour size post-therapy will be $x_S^* + x_D^* + y_S^* + y_D^*$ (see the system of Eq (5.3)) and will be independent of the initial tumour size. When $l_S - a_S$ tends to zero, the probability that the tumour becomes fully infected tends to zero. In Figure 4, as $l_S - a_S$ tends to zero, the line $R_T = 1$ (solid line) tends to infinity.

(III) **Success:** When $R_T \leq 1$, infection completely invades the tumour. As noted previously, 100% infection prevalence is only possible when the net growth rate of infected cancer stem cells is positive, $l_S > a_S$. When $l_S > a_S$ and $R_0 > 1$, as Figure 4 illustrates by an increase in the β_S value, the tumour size is getting smaller and the lowest tumour size is obtained when $\beta_S = a_D b_S(r_S a_S - l_S d_S)/(l_S - a_S)(a_D + l_D)$ (which corresponds to $R_T = 1$). Once β_S reaches $a_D b_S(r_S a_S - l_S d_S)/(l_S - a_S)(a_D + l_D)$, a further increase in β_S no longer impacts the tumour size: for β_S greater than or equal to $a_D b_S(r_S a_S - l_S d_S)/(l_S - a_S)(a_D + l_D)$, the tumour size post-therapy is the same as the tumour size at the steady state E_I. Hence, the tumour size post-therapy is $y_{IS} + y_{ID} = \frac{(l_S - a_S)(a_D + l_D)}{l_S b_S a_D}$, which is independent of the values of β_S and β_D.

3.3. Optimal stem cell specificity

One of the main questions in engineering a virus is when stem cell targeting has an advantage over random or differentiated cell targeting. When infected cells are mitotic and the net growth rate of infected cancer stem cells is positive, as Figure 4 suggests, the minimum tumour size is obtained when $R_T \leq 1$, which corresponds to

$$\beta_S \geq \frac{b_S a_D (r_S a_S - l_S d_S)}{(l_S - a_S)(a_D + l_D)}.$$

This result is not sensitive to the value of β_D, which suggests that when the net growth rate of infected cancer stem cells is positive, the optimal result is obtained by perfect stem cell targeting, in other words, by only targeting stem cells. As Eq (3.9) indicates, when the net growth rate of infected cancer stem cells is negative or zero, R_T is not defined, and only partial infection is possible. In this case, Figure 4 does not provide a clear answer about the optimum stem cell specificity and how average infectivity may affect that. To respond to these concerns, here we reparametrize $\beta_S = p\beta$ and $\beta_D = (1 - p)\beta$, where $0 \leq p \leq 1$ is stem-like specificity and β is the average infectivity. If $p \neq 0.5$, phenotypic heterogeneity is taken into account, whereas if $p = 0.5$, it is not considered, and cells are randomly targeted. If $p > 0.5$, then the engineered oncolytic virus has a higher tendency to infect a stem cell over a differentiated cell. When $p < 0.5$, the oncolytic virus prefers to target differentiated cells over stem cells. When $p = 1$, only stem cells are targeted and when $p = 0$, only differentiated cells are targeted.

In Figure 5, the total tumour size in the steady state as a function of stem cell specificity, p, is plotted for several different values of β. In this figure, for each fixed β, the minimum steady-state tumour size as p varies is denoted by a pink dot. We call this value of p for which the steady-state tumour size is minimised the optimal specificity for the given infectivity rate and denote it by $p_\beta^\star$. The optimal specificity depends on both the infectivity rate and the type of infected cells (mitotic or nonmitotic). Hence, we consider two separate scenarios: 1) nonmitotic infected cells, $l_{S,D} = 0$, Figure 5(a), and 2) mitotic infected cells with negative net growth rate, $l_{S,D} \neq 0$ and $l_S < a_S$, Figure 5(b). Note that in both Figure 5(a),(b), the net growth rate of infected stem cells is negative. Figure 5 illustrates that in both scenarios (mitotic and nonmitotic infected cells), as the average infectivity rate β increases, the minimum steady-state tumour size decreases.

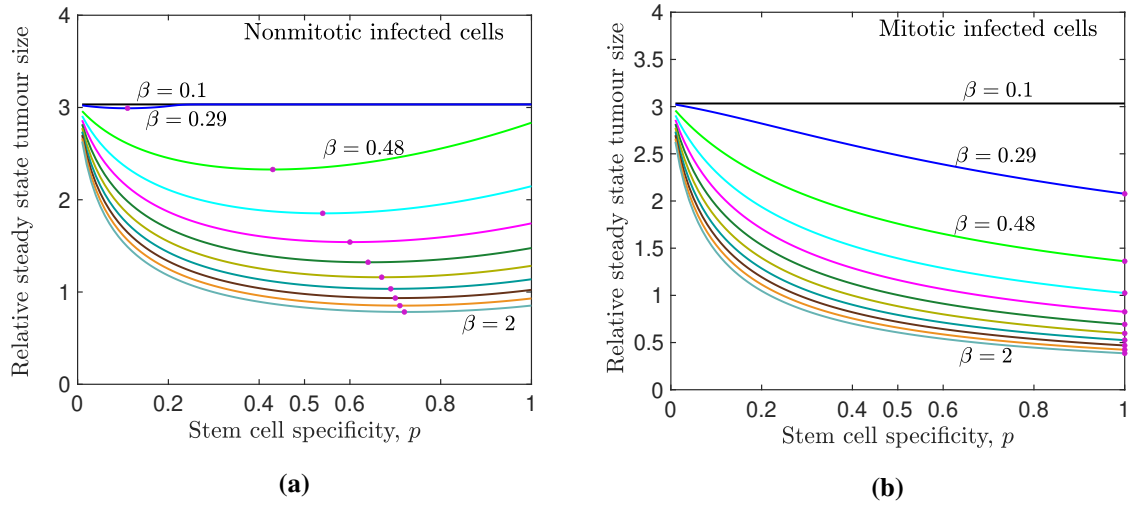

(a) **(b)**

Figure 5. Perfect stem cell targeting is optimal when infected cells are mitotic; (a) nonmitotic infected cells; (b) mitotic infected cells. The specificity, p, is defined by $\beta_S = p\beta, \beta_D = (1-p)\beta$, where $\beta/2$ is the overall infectivity for a uniform system ($p = 0.5$), $\beta_S = \beta_D$. Plots are done for $\beta \in \{0.1, \ldots, 2\}$, with a step size of 0.19. For small infectivity rates, tumour control (weakly) responds to variations in virus-stem cell specificity. Other model parameters are: $r_S = 2, r_D = 4, d_S = 0.3, d_D = 0.6, a_S = d_S + 0.01, a_D = d_D + 0.01, b_S = 1, b_D = 0$. For non-replicating virus, $l_S = l_D = 0$ and for replicating virus, $l_S = 0.25$ and $l_D = 0.5$.

When the infected cells are nonmitotic, $p^\star_\beta$ increases with β, as shown in Figure 5(a). When β is low and p is high, treatment fails, and the steady-state tumour burden remains the same as in the absence of therapy. As infectivity increases, $p^\star_\beta$ passes through $p = 0.5$, and in the high-infectivity regime, stem cell targeting becomes the preferred method. For higher values of β, the minimum steady-state tumour size is not very sensitive to changes in p, and for a wide range of p values, treatment outcomes seem similar. Interestingly, for the range of β used here ($0.1 \le \beta \le 2$), $p^\star_\beta$ is less than one. This means that complete stem cell targeting is not the optimal strategy.

The behaviour described above changes if $l_{S,D} \neq 0$. When infected cells are mitotic, the minimum steady-state tumour size occurs with perfect stem cell targeting. As Figure 5(b) suggests, when p is near zero, treatment has almost no effect on tumour size (no reduction in size) and the tumour size is minimised at $p = 1$. In this figure, the effect of increasing specificity for large infectivity, say $\beta = 2$, is quite strong.

Our numerical simulations suggest that the stem cell fraction increases from the beginning of the therapy if the therapy starts when the tumour size is nearly equal to the tumour size at the E_T steady state and the random targeting regimen is considered (see Figure 3). One might expect that if an oncolytic virus with higher potency in targeting stem cells is used, the stem cell fraction may not increase. However, our numerical simulations show that the same is true under perfect stem cell targeting. Note that cancer differentiated cells originate from cancer stem cells; thus, a decrease in the cancer stem cell population will result in a decrease in the differentiated cell population. An increase in the stem cell fraction implies that the differentiated cell population has declined more substantially than the stem cell population. In the above paragraph, we mentioned that when infected cells' self-renewal and differentiation rates are nonzero, the minimum tumour size is obtained by perfect stem cell targeting.

Under perfect stem cell targeting, treatment reduces the tumour size when β_S is chosen such that $R_0 > 1$. The stem cell fraction increases regardless of the type of infected cells (mitotic or nonmitotic), but the magnitude of increase depends on the mitotic rates of infected cells; increase in these rates results in more tumour shrinkage, but the stem cell fraction becomes larger (see Figure 6 for an illustration).

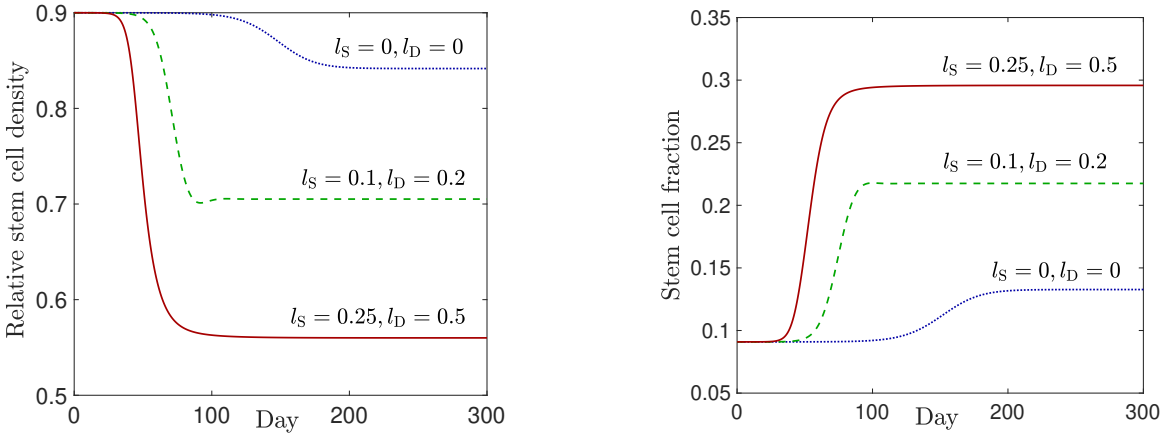

(a) **(b)**

Figure 6. The stem cell fraction increases even under perfect stem cell targeting; (a) stem cell density; (b) stem cell fraction. It is assumed that an oncolytic virus that only targets stem cells is administered. Hence, stem cell specificity p equals one. Three different scenarios are considered; (1) The dotted curve corresponds to nonmitotic infected cells, $l_S = 0, l_D = 0$. (2) The dashed curve corresponds to the case where infected cells are mitotic, and the net growth rate of infected cancer stem cells is negative ($l_S < a_S + d_S$), with $l_S = 0.1$ and $l_D = 0.2$. (3) The solid curve corresponds to the case where infected cells are mitotic, and the net growth rate of infected cancer stem cells is positive ($l_S > a_S + d_S$), with $l_S = 0.25, l_D = 0.5$. Plot (a) demonstrates that when the self-renewal rate and the differentiation rate of infected cancer cells increase, the stem cell density under therapy is reduced. Plot (b) illustrates when the self-renewal rate and the differentiation rate of infected cancer cells increase, stem cell fraction increases. Other model parameters are: $r_S = 1, r_D = 2, d_S = 0.1, d_D = 0.2, a_S = d_S + 0.01, a_D = d_D + 0.01, \beta_S = p\beta, \beta_D = (1-p)\beta, b_S = 1, b_D = 0, \beta = 0.5$.

4. Discussion

Intratumoural heterogeneity is known as a major cause of tumour relapse, recurrence, and failure of many conventional therapies [1, 37, 38]. In fact, most conventional therapies kill differentiated cells, but fail to target cancer stem cells. Due to properties such as self-renewal and quiescence, cancer stem cells are resistant to chemotherapy and radiotherapy [8, 28]. Oncolytic viruses are capable of targeting both quiescent and non-quiescent cancer stem cells and suppressing the growth of cancer stem cells [39–41]. While some in vitro studies report complete eradication of cancer stem cells following oncolytic virotherapy [12, 14], such outcomes are rarely observed in in vivo models [14, 42]. In this paper, our primary goal was to propose a simple mathematical model to analyse the efficiency of targeting cancer stem cells with oncolytic viruses. To do this, we disregarded some complexities related to hierarchical tumour structure, and we also considered some hypotheses related to oncolytic

virotherapy, assumptions (A1)–(A5). Our promising yet simple model agrees with the results of in vitro and in vivo studies of targeting cancer stem cells with oncolytic viruses in that oncolytic viruses can infect all the tumour cells regardless of their phenotypic heterogeneity, reducing the density of both cancer stem cells and differentiated cells. In addition, it agrees with most of the in vivo studies in noting that oncolytic viruses cannot eradicate cancer stem cells (see treatment outcomes (I)–(III)).

One of the most important results of this paper is identifying conditions under which targeting stem cells is more effective than random targeting. Our analysis shows that this depends strongly on the mitotic capability of cancer stem cells (see Section 3.2). If cancer stem cells, after becoming infected, cannot self-renew or differentiate, then targeting stem cells (even with higher specificity) with oncolytic viruses does not improve the treatment efficiency (see Figures 4 and 5). In fact, in this scenario, the average infectivity rate has more effect than mitotic capability of infected cancer stem cells on optimal tumour size post-therapy. As numerical simulations illustrate, when the average infectivity increases, treatment leads to greater tumour shrinkage (see Figures 3–5). When cancer stem cells are mitotic, meaning that they can self-renew and differentiate, targeting cancer stem cells is more effective than random targeting or only targeting differentiated cells. When cancer stem cells are mitotic, the smallest tumour size is achieved under perfect stem cell targeting (see Figure 5 for an illustration). Moreover, when the net growth rate of infected cancer stem cells is positive, there exists an optimal infectivity rate at which therapy minimizes the tumour size (see inequality (3.10)).

The success of oncolytic viral therapy depends heavily on the extent to which infection can invade the tumour [24]. Hence, the basic reproduction number R_0 is a valuable marker to know when virotherapy starts to work. We calculated R_0, and showed that therapy is only effective when $R_0 > 1$: this also gives a linear constraint on the infectivity rates of cancer stem cells and cancer differentiated cells, meaning it formulates to which extent cancer stem cells and cancer differentiated cells must be targeted to see long-term tumour shrinkage (see Theorem 2).

To ensure consistency across simulations, we have selected the virus-free steady state as the initial condition. It is important to note that our results, such as constraints on the parameter space under which infection invades the tumour or the increase in the stem cell fraction under treatment, are general and do not depend on specific initial conditions. In typical in vivo experiments, human cancer cells are often engrafted into immunodeficient (nude) mice. Researchers then wait until the tumour reaches a certain size before administering the oncolytic virus [43, 44]. For our simulations, we assume that the tumour is allowed to grow to its maximum carrying capacity prior to the administration of the oncolytic virus; this is equivalent to assuming that the tumour is in its virus-free steady state before the start of the treatment.

The quasi-steady-state assumption (A1) regarding viral dynamics has previously been adopted by Komarova and Wodarz [36, 45] in the context of mathematical modelling of oncolytic virotherapy. Relaxing this assumption necessitates the use of a five-compartment model that includes an explicit equation describing the temporal dynamics of free virus. Importantly, our key findings, such as when the perfect stem cell targeting regimen leads to the minimum tumour size when infected cells are mitotic, remain valid under this extended modelling framework. However, incorporating the interaction between free virus and cancer cells would allow for the investigation of virus-specific immune responses and their impact on overall treatment outcomes. Note that, for simplicity, interaction with the immune response is not considered in this work. Nevertheless, in the presence of an immune response, both the partial infection steady state and the 100% infection prevalence are

observable. We have demonstrated this in an alternative modelling framework [46, see Chapter 3], and similar results have been reported in other studies [36, 47].

As mentioned in the introduction, cancer stem cells are located in cancer stem cell niches. In a recent study of glioblastoma, Liu et al. [48] showed that different cancer phenotypes are localized in separate niches and regions of the tumour. These localizations may affect the way that the virus spreads and infects different cell types. Our model does not take such spatial heterogeneity into account. Targeting stem cells with oncolytic viruses is very challenging due to their clustering in the cancer stem cell niche. A mathematical model that considers such a spatial heterogeneity could shed more light on capturing the efficacy of targeting stem cells with oncolytic viruses.

Infection can affect the cell regulation machinery. There is controversy about how stem cell hierarchy gets affected if a cell in any hierarchy level becomes infected. For example, in the case of human papillomavirus (HPV), researchers using in vivo models have shown that if a stem cell gets infected, both of its daughter cells will get infected [49]. However, if a cell gets infected at a lower hierarchy level, both daughter cells will be uninfected [49]. In the case of human immunodeficiency virus (HIV), in vivo models have shown that if a stem cell gets infected then the daughter cells will be infected [50]. An in vitro study of hepatitis B virus (HBV) shows that both daughter cells of an infected cell are uninfected [51]. In another study, to understand the clearance of acute infection in the case of HBV, the authors made three hypotheses: (1) Both daughter cells of an infected cell are infected (2) One daughter cell is infected, and the other daughter cell is uninfected (3) Both daughter cells of an infected cell are uninfected [52]. They introduced mathematical models corresponding to each hypothesis and fitted the models to the longitudinal patient data. The closest fit corresponded to the hypothesis that both daughter cells of an infected cell are uninfected. In this paper, we assumed both daughter cells of an infected cell are infected. All our results in this paper are appropriate for a virus that, when it infects a stem cell, both of its daughter cells are infected.

The tumour microenvironment and hierarchical structure within a tumour are very complex. The hierarchical structure starts from a stem cell at the top of the hierarchy and ends in the last row of fully differentiated cells. Stem cells may self-renew or differentiate symmetrically or asymmetrically. Here, for simplicity, we only considered self-renewal and symmetric differentiation. Our model can be extended to a full hierarchical model such as the one discussed by Werner et al. [53].

5. Methods

5.1. Closed form of the interior equilibrium

Let $E_{\mathrm{p}} = (x_{\mathrm{S}}^*, x_{\mathrm{D}}^*, y_{\mathrm{S}}^*, y_{\mathrm{D}}^*)$ be the interior equilibrium. Hence,

$$r_{\mathrm{S}}(1 - b_{\mathrm{S}}(x_{\mathrm{S}}^* + y_{\mathrm{S}}^*)) - d_{\mathrm{S}} - \beta_{\mathrm{S}}(y_{\mathrm{S}}^* + y_{\mathrm{D}}^*) = 0, \tag{5.1a}$$

$$r_{\mathrm{D}}x_{\mathrm{S}}^* - d_{\mathrm{D}}x_{\mathrm{D}}^* - \beta_{\mathrm{D}}x_{\mathrm{D}}^*(y_{\mathrm{S}}^* + y_{\mathrm{D}}^*) = 0, \tag{5.1b}$$

$$l_{\mathrm{S}}y_{\mathrm{S}}^*(1 - b_{\mathrm{S}}(x_{\mathrm{S}}^* + y_{\mathrm{S}}^*)) - a_{\mathrm{S}}y_{\mathrm{S}}^* + \beta_{\mathrm{S}}x_{\mathrm{S}}^*(y_{\mathrm{S}}^* + y_{\mathrm{D}}^*) = 0, \tag{5.1c}$$

$$l_{\mathrm{D}}y_{\mathrm{S}}^* - a_{\mathrm{D}}y_{\mathrm{D}}^* + \beta_{\mathrm{D}}x_{\mathrm{D}}^*(y_{\mathrm{S}}^* + y_{\mathrm{D}}^*) = 0. \tag{5.1d}$$

Upon introducing $T = y_{\mathrm{S}}^* + y_{\mathrm{D}}^*$, the above set of equations simplifies to

$$r_{\mathrm{S}}(1 - b_{\mathrm{S}}(x_{\mathrm{S}}^* + y_{\mathrm{S}}^*)) - d_{\mathrm{S}} - \beta_{\mathrm{S}}T = 0, \tag{5.2a}$$

$$r_D x_S^* - d_D x_D^* - \beta_D x_D^* T = 0, \tag{5.2b}$$
$$l_S y_S^*(1 - b_S(x_S^* + y_S^*)) - a_S y_S^* + \beta_S x_S^* T = 0, \tag{5.2c}$$
$$l_D y_S^* - a_D(T - y_S^*) + \beta_D x_D^* T = 0. \tag{5.2d}$$

By solving the above system of equations the closed forms for x_S^*, x_D^*, y_S^*, and y_D^* are obtained as follows.

$$x_S^* = \frac{(r_S - d_S - \beta_S T)(a_S r_S - l_S d_S - l_S \beta_S T)}{b_S r_S((r_S - l_S)\beta_S T + a_S r_S - l_S d_S)}, \tag{5.3a}$$
$$x_D^* = x_S^* \frac{r_D}{\beta_D T + d_D}, \tag{5.3b}$$
$$y_S^* = \frac{\beta_S T(r_S - d_S - \beta_S T)}{b_S((r_S - l_S)\beta_S T + a_S r_S - l_S d_S)}, \tag{5.3c}$$
$$y_D^* = T - y_S^*, \tag{5.3d}$$

where T is a positive root of the quadratic $Q(T)$, shown below.

$$Q(T) = A\ T^2 + B\ T + C, \tag{5.4}$$

where A, B, and C are defined as,

$$A := \beta_S \beta_D \Big(\beta_S((l_D + a_D)r_S - r_D l_S) + b_S a_D r_S(r_S - l_S)\Big), \tag{5.5a}$$
$$B := d_D r_S(l_D + a_D)\beta_S^2 + \Big(((r_S - d_S)(r_D l_S - (l_D + a_D)r_S) + r_D(r_S a_S - l_S d_S))\beta_D \tag{5.5b}$$
$$+ b_S d_D r_S a_D(r_S - l_S)\Big)\beta_S + b_S a_D r_S \beta_D(r_S a_S - l_S d_S),$$
$$C := -(a_D + l_D)(r_S - d_S) r_S d_D \beta_S + (a_S r_S - d_S l_S)\Big(b_S d_D a_D r_S - \beta_D r_D(r_S - d_S)\Big). \tag{5.5c}$$

Note that $Q(T)$ has at most two positive roots. Hence, there could exist at most two positive interior equilibria. Under the assumption given in parts (III) and (IV) of Theorem 1, there exists a unique positive interior equilibrium. In that case T can be found from below.

$$T = -\frac{B}{2A} + \sqrt{\left(\frac{B}{2A}\right)^2 - \frac{C}{A}}, \quad \text{where } A > 0 \text{ and } C < 0.$$

5.2. Proof of Theorem 1

Proof of (I). Recall $E_T = (\frac{1}{b_S}(1 - \frac{d_S}{r_S}), \frac{r_D}{b_S d_D}(1 - \frac{d_S}{r_S}), 0, 0)$. Based on assumption (A4), $d_S < r_S$, both nonzero components of E_T are positive.

Proof of (II). $E_I = (0, 0, \frac{1}{b_S}(1 - \frac{a_S}{l_S}), \frac{l_D}{b_S a_D}(1 - \frac{a_S}{l_S}))$. When $a_S < l_S$ and $l_{S,D} \neq 0$, both nonzero components of E_I are positive.

Proof of (III). Suppose $a_S < l_S$, $1 < \dfrac{r_D}{a_D + l_D} < \dfrac{r_S}{l_S}$, and

$$\frac{a_S r_S - d_S l_S}{a_D + l_D} \cdot \frac{b_S d_D a_D r_S - \beta_D r_D(r_S - d_S)}{r_S d_D(r_S - d_S)} < \beta_S < \frac{b_S a_D(r_S a_S - l_S d_S)}{(l_S - a_S)(a_D + l_D)}. \tag{5.6}$$

We show E_p is unique and strictly positive under these assumptions, where $E_p = (x_S^*, x_D^*, y_S^*, y_D^*)$, see the system of Eqs (5.3). For the interior steady state E_p to be positive, x_S^*, x_D^*, y_S^*, and y_D^* must be positive when T is a positive root of the quadratic $Q(T) = A\ T^2 + B\ T + C$.

In Eq (5.3c), the denominator is always positive according to assumption (A5), $l_S < r_S$ and $d_S < a_S$. Therefore, $a_S r_S - d_S l_S > 0$ and $r_S - l_S > 0$. Since the denominator in Eq (5.3c) is always positive, for y_S^* to be positive, it suffices that the numerator be positive. Hence, $r_S - d_S - \beta_S T > 0$.

Similarly, in Eq (5.3a), the denominator is positive. Hence, for x_S^* to be positive, the numerator must also be positive; that is,

$$(r_S - d_S - \beta_S T)(a_S r_S - l_S d_S - l_S \beta_S T) > 0.$$

As we mentioned above, y_S^* is positive if and only if $r_S - d_S - \beta_S T > 0$. Therefore, x_S^* and y_S^* are positive if and only if $r_S - d_S - \beta_S T > 0$ and $a_S r_S - l_S d_S - l_S \beta_S T > 0$. Hence, x_S^* and y_S^* are positive if and only if

$$T < \min\{\frac{r_S - d_S}{\beta_S}, \frac{r_S a_S - l_S d_S}{l_S \beta_S}\}.$$

According to the theorem's assumption, $a_S < l_S$, $\frac{a_S}{l_S} < 1$. Hence, $\frac{a_S}{l_S} r_S < r_S$. Thus, $\frac{r_S \frac{a_S}{l_S} - d_S}{\beta_S} < \frac{r_S - d_S}{\beta_S}$. Therefore,

$$T < \min\{\frac{r_S - d_S}{\beta_S}, \frac{r_S a_S - l_S d_S}{l_S \beta_S}\} = \frac{r_S a_S - l_S d_S}{l_S \beta_S}. \tag{5.7}$$

From the system of Eq (5.3), when x_S^* is positive, x_D^* is also positive. Moreover, for y_D^* to be positive,

$$\frac{(r_S - d_S)\beta_S - b_S(a_S r_S - l_S d_S)}{\beta_S + b_S(r_S - l_S)} < T. \tag{5.8}$$

Therefore, by the inequalities (5.7) and (5.8), x_S^*, x_D^*, y_S^*, and y_D^* are all positive if and only if the quadratic Q has a positive root T^* such that

$$\frac{(r_S - d_S)\beta_S - b_S(a_S r_S - l_S d_S)}{\beta_S + b_S(r_S - l_S)} < T^* < \frac{r_S a_S - l_S d_S}{l_S \beta_S}. \tag{5.9}$$

Under the assumption of the theorem ($\frac{r_D}{a_D + l_D} < \frac{r_S}{l_S}$), the leading coefficient A of the quadratic Q is positive. By the left-hand inequality of (5.6), $C = Q(0) < 0$. Hence, the quadratic Q has a unique positive root T^*, given below.

$$T^* = -\frac{B}{2A} + \sqrt{(\frac{B}{2A})^2 - \frac{C}{A}}. \tag{5.10}$$

To complete the proof, we must show that T^* satisfies inequality (5.9). To show this, we first evaluate the quadratic Q at the bounds specified in inequality (5.9).

$$Q(\frac{r_S a_S - l_S d_S}{l_S \beta_S}) = \frac{r_S^2}{\beta_S l_S^2}(b_S a_D (r_S a_S - l_S d_S) - (l_S - a_S)(l_D + a_D)\beta_S)((r_S a_S - l_S d_S)\beta_D + l_S d_D \beta_S).$$

$$Q(\frac{(r_S - d_S)\beta_S - b_S(a_S r_S - l_S d_S)}{\beta_S + b_S(r_S - l_S)}) = \beta_D(r_D \beta_S (l_S - a_S) - b_S(a_S r_S - l_S d_S)(r_D - l_D)) - l_D \beta_S \big(\beta_D(r_S - d_S)$$

$$+ d_D(b_S(r_S - l_S) + \beta_S)\Big).$$

By the right-hand inequality of (5.6), $\beta_S < \frac{b_S a_D(r_S a_S - l_S d_S)}{(l_S - a_S)(l_D + a_D)}$. Therefore, $Q(\frac{r_S a_S - l_S d_S}{l_S \beta_S}) > 0$. By the assumption of the theorem ($a_D + l_D < r_D$),

$$\beta_S < \frac{b_S(r_S a_S - l_S d_S)a_D}{(l_S - a_S)(a_D + l_D)} < \frac{b_S(r_S a_S - l_S d_S)(r_D - l_D)}{(l_S - a_S)r_D}.$$

Therefore, $Q(\frac{(r_S - d_S)\beta_S - b_S(a_S r_S - l_S d_S)}{\beta_S + b_S(r_S - l_S)}) < 0$. Since $Q(\frac{(r_S - d_S)\beta_S - b_S(a_S r_S - l_S d_S)}{\beta_S + b_S(r_S - l_S)})Q(\frac{r_S a_S - l_S d_S}{l_S \beta_S}) < 0$ and Q is a continuous function of T, by the intermediate value theorem, Q has a root that satisfies the inequality (5.9); since this root satisfies inequality (5.9), it must be positive. Since T^*, given by Eq (5.10), is the only positive root of the quadratic Q, then, T^* satisfies inequality (5.9).

Proof of (IV). Suppose $l_S = l_D = 0$ and $\beta_S > \frac{a_S\left(a_D d_D b_S r_S - \beta_D r_D(r_S - d_S)\right)}{a_D d_D(r_S - d_S)}$. When $l_S = l_D = 0$, the set of Eq (5.3) can be rewritten as

$$x_S^* = \frac{(r_S - d_S - \beta_S T)a_S}{b_S r_S(T\beta_S + a_S)}, \tag{5.11a}$$

$$x_D^* = \frac{r_D}{\beta_D T + d_D} x_S^*, \tag{5.11b}$$

$$y_S^* = \frac{\beta_S T}{a_S} x_S^*, \tag{5.11c}$$

$$y_D^* = \frac{T(T\beta_S^2 + (Tb_S r_S + d_S - r_S)\beta_S + b_S a_S r_S)}{b_S r_S(T\beta_S + a_S)}, \tag{5.11d}$$

where T is a positive root of the following quadratic, $Q_1(T) = A_1 T^2 + B_1 T + C_1$, where
$A_1 := a_D \beta_D \beta_S(b_S r_S + \beta_S)$,
$B_1 := a_D d_D \beta_S^2 + \Big((b_S r_S d_D - (r_S - d_S)\beta_D)a_D + a_S r_D \beta_D\Big)\beta_S + a_D a_S b_S r_S \beta_D$,
$C_1 := a_S(a_D d_D b_S r_S - \beta_D r_D(r_S - d_S)) - a_D d_D(r_S - d_S)\beta_S$.

Note that A_1 is always positive. Under the assumption $\beta_S > \frac{a_S\left(a_D d_D b_S r_S - \beta_D r_D(r_S - d_S)\right)}{a_D d_D(r_S - d_S)}$, $C_1 < 0$. Since $A_1 > 0$ and $C_1 < 0$ the quadratic Q_1 has a unique positive root $T_1^* = \frac{-B_1}{2A_1} + \sqrt{(\frac{B_1}{2A_1})^2 - \frac{C_1}{A_1}}$. For the interior steady state $E_p = (x_S^*, x_D^*, y_S^*, y_D^*)$ to exist, we should show that for $T = T_1^*$, all the components of E_p are positive.

From the set of Eq (5.11), when x_S^* is positive, x_D^*, y_S^* are positive. Therefore, a positive steady state exists if and only if for $T = T_1^*$, x_S^* and y_D^* are both positive.

$x_S^* > 0$ if and only if $T_1^* < \dfrac{r_S - d_S}{\beta_S}$.

$y_D^* > 0$ if and only if $\dfrac{(r_S - d_S)\beta_S - a_S b_S r_S}{\beta_S(b_S r_S + \beta_S)} < T_1^*$.

Therefore, there exists an interior steady state if and only if there exists a positive root T of the quadratic $Q_1(T)$ such that

$$\frac{(r_S - d_S)\beta_S - a_S b_S r_S}{\beta_S(b_S r_S + \beta_S)} < T < \frac{r_S - d_S}{\beta_S}. \tag{5.12}$$

To complete the proof, we must show that T_1^* satisfies inequality (5.12). To show this, we first evaluate the quadratic Q_1 at the bounds specified in inequality (5.12).

$$Q_1\left(\frac{(r_S - d_S)\beta_S - a_S b_S r_S}{\beta_S(b_S r_S + \beta_S)}\right) = -\frac{a_S r_D \beta_D b_S r_S (a_S + r_S - d_S)}{\beta_S + b_S r_S}.$$

$$Q_1\left(\frac{r_S - d_S}{\beta_S}\right) = \frac{b r_S^2 (a_S + r_S - d_S)(\beta_D(r_S - d_S) + \beta_S d_D) a_D}{\beta_S}.$$

By assumption (A4), $d_S < r_S$, $Q_1(\frac{(r_S-d_S)\beta_S - a_S b_S r_S}{\beta_S(b_S r_S+\beta_S)}) < 0$, and $Q_1(\frac{r_S-d_S}{\beta_S}) > 0$. Since $Q_1(T)$ is a continuous function of T, and $Q_1(\frac{(r_S-d_S)\beta_S - a_S b_S r_S}{\beta_S(b_S r_S+\beta_S)})Q_1(\frac{r_S-d_S}{\beta_S}) < 0$, by the intermediate value theorem Q_1 has a positive root in the interval $\left(\frac{(r_S-d_S)\beta_S - a_S b_S r_S}{\beta_S(b_S r_S+\beta_S)}, \frac{r_S-d_S}{\beta_S}\right)$. Since T_1^* is the only positive root of $Q_1(T)$,

$$\frac{(r_S - d_S)\beta_S - a_S b_S r_S}{\beta_S(b_S r_S + \beta_S)} < T_1^* < \frac{r_S - d_S}{\beta_S}.$$

□

5.3. The basic reproduction number and proof of lemma 1

Here we use the method proposed by van den Driessche and Watmough in [25] to calculate the basic reproduction number R_0.

Recall the basic reproduction number represents the number of new infected cells that an infected cell produces in its lifetime when almost all the cells are susceptible to infection. Therefore, when calculating the basic reproduction number, we are only interested in the dynamics of cancer cells in infected compartments. From Model (2.3),

$$(\dot{y_S}, \dot{y_D}) = \mathscr{F}_I - \mathscr{V}_I, \tag{5.13}$$

where $\mathscr{F}_I$ refers to the appearance of new infections and $\mathscr{V}_I$ refers to the removal of infected cells. Therefore,

$$\mathscr{F}_I = \Big(l_S y_S(1 - bs(x_S + y_S)) + \beta_S x_S(y_S + y_D), \tag{5.14a}$$
$$l_D y_S + \beta_D x_D(y_S + y_D)\Big).$$
$$\mathscr{V}_I = (a_S y_S, a_D y_D). \tag{5.14b}$$

To calculate the next generation matrix $\mathscr{N}_I$, we should calculate Jacobians of $\mathscr{F}_I$ and $\mathscr{V}_I$, with respect to y_S and y_D at the infection-free steady state $E_T = (x_{TS}, x_{TD}, 0, 0)$ (in other words, the steady state in which almost all the cells are susceptible to infection).

$$F_I = \frac{\partial \mathscr{F}_I}{\partial(y_S, y_D)} = \begin{bmatrix} l_S\dfrac{d_S}{r_S} + \beta_S x_{TS} & \beta_S x_{TS} \\ l_D + \beta_D x_{TD} & \beta_D x_{TD} \end{bmatrix}, \tag{5.15a}$$

$$V_I = \frac{\partial \mathscr{V}_I}{\partial(y_S, y_D)} = \begin{bmatrix} a_S & 0 \\ 0 & a_D \end{bmatrix}. \tag{5.15b}$$

$\mathscr{N}_I = F_I V_I^{-1}$, hence,

$$\mathscr{N}_I = \begin{bmatrix} \frac{l_S}{a_S}\frac{d_S}{r_S} + \frac{\beta_S x_{TS}}{a_S} & \frac{\beta_S x_{TS}}{a_D} \\ \frac{l_D}{a_S} + \frac{\beta_D x_{TD}}{a_S} & \frac{\beta_D x_{TD}}{a_D} \end{bmatrix}. \tag{5.16}$$

Proof of Lemma 1. The basic reproduction number is the spectral radius of $\mathscr{N}_I$. The spectral radius of a square matrix is the maximum of absolute values (magnitudes) of its eigenvalues. Since $\mathscr{N}_I$ is a matrix with positive entries, by the Perron-Forbenius theorem [54], the spectral radius of $\mathscr{N}_I$ is one of its eigenvalues. The eigenvalues of $\mathscr{N}_I$ are zeros of the quadratic $\lambda^2 - \text{tr}(\mathscr{N}_I)\lambda + \det(\mathscr{N}_I)$. Since $\text{tr}(\mathscr{N}_I) > 0$, the eigenvalue of $\mathscr{N}_I$ with the biggest magnitude is the following.

$$R_0 = \frac{\text{tr}(\mathscr{N}_I)}{2} + \sqrt{\left(\frac{\text{tr}(\mathscr{N}_I)}{2}\right)^2 - \det(\mathscr{N}_I)}. \tag{5.17}$$

5.4. Proof of Theorem 2

By Eq (5.17), $R_0 > 1$ if and only if

$$\sqrt{\left(\frac{\text{tr}(\mathscr{N}_I)}{2}\right)^2 - \det(\mathscr{N}_I)} > 1 - \frac{\text{tr}(\mathscr{N}_I)}{2}. \tag{5.18}$$

If $\text{tr}(\mathscr{N}_I)$ is greater than two, inequality (5.18) holds. The trace of $\mathscr{N}_I$ is greater than two if and only if

$$\beta_S > \frac{b_S(2a_S r_S - d_S l_S)}{r_S - d_S} - \beta_D \frac{r_D a_S}{a_D d_D}. \tag{5.19}$$

Let L_2 denote the line $\beta_S = \frac{b_S(2a_S r_S - d_S l_S)}{r_S - d_S} - \beta_D \frac{r_D a_S}{a_D d_D}$; this line is shown by a dash line in Figure 7. Hence, in the area shaded yellow (above line L_2) in Figure 7, R_0 is greater than one.

Assume the trace of $\mathscr{N}_I$ is smaller than two. Squaring both sides of inequality 5.18 yields

$$1 - \text{tr}(\mathscr{N}_I) + \det(\mathscr{N}_I) < 0. \tag{5.20}$$

Since $\det(\mathscr{N}_I) = \frac{(r_S - d_S)(\beta_D l_S d_S r_D - \beta_S l_D d_D r_S)}{b_S d_D a_D a_S r_S^2}$ and $\text{tr}(\mathscr{N}_I) = \frac{d_S l_S}{a_S r_S} + \frac{r_S - d_S}{b_S r_S}\left(\frac{\beta_S}{a_S} + \frac{\beta_D r_D}{a_D d_D}\right)$, inequality (5.20) can be written as

$$\beta_S > \left(\frac{b_S a_D}{r_S - d_S} - \beta_D \frac{r_D}{r_S d_D}\right)\frac{r_S a_S - l_S d_S}{l_D + a_D}. \tag{5.21}$$

Let L_1 denote the line $\beta_S = \left(\frac{b_S a_D}{r_S - d_S} - \beta_D \frac{r_D}{r_S d_D}\right)\frac{r_S a_S - l_S d_S}{l_D + a_D}$.
Since the value of β_D (β_S) for which L_2 intercepts the β_D (β_S) axis is always greater than the value of β_D (β_S) for which L_1 intercepts the β_D (β_S) axis, line L_2 in the $\beta_D - \beta_S$ plane is always above line L_1,

as shown in Figure 7. In the area shaded green in Figure 7, the trace of $\mathscr{N}_{\mathrm{I}}$ is smaller than two and inequality (5.18) holds. Hence, in the area shaded green in Figure 7, R_0 is greater than one.

When the trace of $\mathscr{N}_{\mathrm{I}}$ is equal to two, inequality 5.18 holds. Note that by the Perron-Forbenius theorem [54], the square root on the right-hand side of inequality 5.18 is defined.

Therefore, R_0 is greater than one in both areas shaded yellow and green, and along the dashed line in Figure 7, that is, the area above line L_1. The area above line L_1 corresponds to the parameter space in which inequality (5.21) holds. Hence, $R_0 > 1$ if and only if inequality (5.21) holds. □

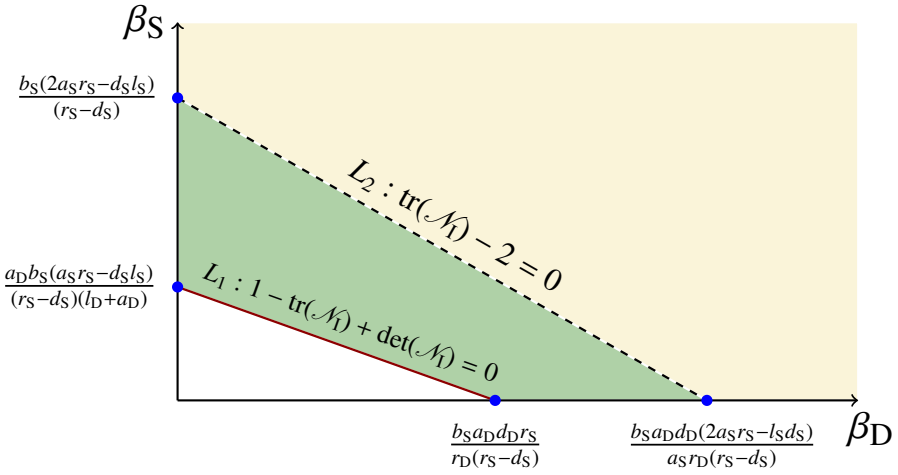

Figure 7. R_0 is greater than one in the shaded areas and along line L_2. Above line L_1, $1 - \mathrm{tr}(\mathscr{N}_{\mathrm{I}}) + \det(\mathscr{N}_{\mathrm{I}})$ is negative. Above line L_2, the trace of $\mathscr{N}_{\mathrm{I}}$ is greater than two and below line L_2, the trace of $\mathscr{N}_{\mathrm{I}}$ is less than two. In the shaded areas and along line L_2, inequality (5.18) holds.

5.5. The reproduction number of uninfected cancer cells

Similar to Section 5.3, we use the method given by van den Driessche and Watmough in [25] to calculate the reproduction number R_{T} of uninfected cancer cells.

Recall the reproduction number of uninfected cancer cells is the number of new uninfected cancer cells that an uninfected cancer cell produces during its lifetime when almost all the tumour cells are already infected. Therefore, in this case only the dynamics of uninfected cancer cells over time is important. Hence, we only consider the target space, the surface $x_{\mathrm{S}} - x_{\mathrm{D}}$. We rewrite the model as follows:

$$(\dot{x_{\mathrm{S}}}, \dot{x_{\mathrm{D}}}) \quad = \quad \mathscr{F}_{\mathrm{T}} - \mathscr{V}_{\mathrm{T}}, \tag{5.22}$$

where $\mathscr{F}_{\mathrm{T}}$ refers to the growth in the population of uninfected cancer cells and $\mathscr{V}_{\mathrm{T}}$ refers to the cell removal from the compartments of uninfected cancer cells. Thus,

$$\mathscr{F}_{\mathrm{T}} = \Big(r_{\mathrm{S}}x_{\mathrm{S}}(1 - b_{\mathrm{S}}(x_{\mathrm{S}} + y_{\mathrm{S}})), r_{\mathrm{D}}x_{\mathrm{S}}\Big), \tag{5.23}$$

$$\mathscr{V}_{\mathrm{T}} = (d_{\mathrm{S}}x_{\mathrm{S}} + \beta_{\mathrm{S}}x_{\mathrm{S}}(y_{\mathrm{S}} + y_{\mathrm{D}}), d_{\mathrm{D}}x_{\mathrm{D}} + \beta_{\mathrm{D}}x_{\mathrm{D}}(y_{\mathrm{S}} + y_{\mathrm{D}})). \tag{5.24}$$

Next, the Jacobians of $\mathscr{F}_{\mathrm{T}}$ and $\mathscr{V}_{\mathrm{T}}$ with respect to x_{S} and x_{D} are calculated at the steady state $E_{\mathrm{I}} =$

$(0, 0, y_{\mathrm{IS}}, y_{\mathrm{ID}})$.

$$F_T = \frac{\partial \mathscr{F}_T}{\partial(x_{\mathrm{S}}, x_{\mathrm{D}})}, \tag{5.25}$$

$$V_T = \frac{\partial \mathscr{V}_T}{\partial(x_{\mathrm{S}}, x_{\mathrm{D}})}. \tag{5.26}$$

Hence,

$$F_T = \begin{bmatrix} r_{\mathrm{S}}\dfrac{a_{\mathrm{S}}}{l_{\mathrm{S}}} & 0 \\ r_{\mathrm{D}} & 0 \end{bmatrix}, \tag{5.27}$$

$$V_T = \begin{bmatrix} d_{\mathrm{S}} + \beta_{\mathrm{S}}(y_{\mathrm{IS}} + y_{\mathrm{ID}}) & 0 \\ 0 & d_{\mathrm{D}} + \beta_{\mathrm{D}}(y_{\mathrm{IS}} + y_{\mathrm{ID}}) \end{bmatrix}. \tag{5.28}$$

The next generation matrix $\mathscr{N}_{\mathrm{T}}$ of target cells is given by $\mathscr{N}_{\mathrm{T}} = F_T(V_T)^{-1}$, so

$$\mathscr{N}_{\mathrm{T}} = \begin{bmatrix} \left(\dfrac{r_{\mathrm{S}}}{d_{\mathrm{S}} + \beta_{\mathrm{S}}(y_{\mathrm{IS}} + y_{\mathrm{ID}})}\right)\dfrac{a_{\mathrm{S}}}{l_{\mathrm{S}}} & 0 \\ \dfrac{r_{\mathrm{D}}}{d_{\mathrm{S}} + \beta_{\mathrm{S}}(y_{\mathrm{IS}} + y_{\mathrm{ID}})} & 0 \end{bmatrix}. \tag{5.29}$$

R_{T} is the spectral radius of $\mathscr{N}_{\mathrm{T}}$. It is trivial that eigenvalues of $\mathscr{N}_{\mathrm{T}}$ are 0 and $\left(\dfrac{r_{\mathrm{S}}}{d_{\mathrm{S}} + \beta_{\mathrm{S}}(y_{\mathrm{IS}} + y_{\mathrm{ID}})}\right)\dfrac{a_{\mathrm{S}}}{l_{\mathrm{S}}}$. Therefore,

$$R_{\mathrm{T}} = \left(\frac{r_{\mathrm{S}}}{d_{\mathrm{S}} + \beta_{\mathrm{S}}(y_{\mathrm{IS}} + y_{\mathrm{ID}})}\right)\frac{a_{\mathrm{S}}}{l_{\mathrm{S}}}. \tag{5.30}$$

Use of AI tools declaration

The authors declare they have not used Artificial Intelligence (AI) tools in the creation of this article.

Acknowledgments

This work was partially supported by the Natural Sciences and Engineering Research Council of Canada (NSERC; RGPIN-2017-05760) and the Canadian Institutes of Health Research (CIHR), the Mathematical Modeling of the COVID-19 Task Force.

Conflict of interest

The authors declare there is no conflict of interest.

References

1. S. Turajlic, A. Sottoriva, T. Graham, C. Swanton, Resolving genetic heterogeneity in cancer, *Nat. Rev. Genet.*, **20** (2019), 404–416. https://doi.org/10.1038/s41576-019-0114-6
2. N. McGranahan, C. Swanton, Biological and therapeutic impact of intratumor heterogeneity in cancer evolution, *Cancer Cell*, **27** (2015), 15–26. https://doi.org/10.1016/j.ccell.2014.12.001
3. A. Marusyk, V. Almendro, K. Polyak, Intra-tumour heterogeneity: A looking glass for cancer? *Nat. Rev. Cancer*, **12** (2012), 323–334. https://doi.org/10.1038/nrc3261
4. B. Beck, C. Blanpain, Unravelling cancer stem cell potential, *Nat. Rev. Cancer*, **13** (2013), 727–738. https://doi.org/10.1038/nrc3597
5. P. Valent, D. Bonnet, R. De Maria, T. Lapidot, M. Copland, J. V. Melo, et al., Cancer stem cell definitions and terminology: The devil is in the details, *Nat. Rev. Cancer*, **12** (2012), 767–775. https://doi.org/10.1038/nrc3368
6. S. Vinogradov, X. Wei, Cancer stem cells and drug resistance: the potential of nanomedicine, *Nanomedicine*, **7** (2012), 597–615. https://doi.org/10.2217/nnm.12.22
7. T. Reya, S. J. Morrison, M. F. Clarke, I. L. Weissman, Stem cells, cancer, and cancer stem cells, *Nature*, **414** (2001), 105–111. https://doi.org/10.1038/35102167
8. N. Picco, R. A. Gatenby, A. R. A. Anderson, Stem cell plasticity and niche dynamics in cancer progression, *IEEE Trans. Biomed. Eng.*, **64** (2017), 528–537. https://doi.org/10.1109/TBME.2016.2607183
9. W. Yu, Z. Wang, C. Fong, D. Liu, T. Yip, S. Au, et al., Chemoresistant lung cancer stem cells display high DNA repair capability to remove cisplatin-induced DNA damage, *Br. J. Pharmacol.*, **174** (2017), 302–313. https://doi.org/10.1111/bph.13690
10. A. Schulz, F. Meyer, A. Dubrovska, K. Borgmann, Cancer stem cells and radioresistance: DNA repair and beyond, *Cancers*, **11** (2019), 862. https://doi.org/10.3390/cancers11060862
11. D. T. Curiel, P. Fisher, *Applications of Viruses for Cancer Therapy*, Academic Press, 2012.
12. M. Eriksson, K. Guse, G. Bauerschmitz, P. Virkkunen, M. Tarkkanen, M. Tanner, et al., Oncolytic adenoviruses kill breast cancer initiating $CD44^{+}$ $CD24^{-/Low}$ cells, *Mol. Ther.*, **15** (2007), 2088–2093. https://doi.org/10.1038/sj.mt.6300300
13. T. Liu, D. Kirn, Targeting the untargetable: oncolytic virotherapy for the cancer stem cell, *Mol. Ther.*, **15** (2007), 2060–2061. https://doi.org/10.1038/sj.mt.6300337
14. G. J. Bauerschmitz, T. Ranki, L. Kangasniemi, C. Ribacka, M. Eriksson, M. Porten, et al., Tissue-specific promoters active in $CD44^{+}$ $CD24^{-/low}$ breast cancer cells, *Cancer Res.*, **68** (2008), 5533–5539. https://doi.org/10.1158/0008-5472.CAN-07-5288
15. M. Sagara, H. Inoue, S. Miyamoto, C. Sakamoto, Y. Nakano, K. Takayama, et al., CVB3 infection elicits potent oncolytic activity against lung cancer stemcells, *Mol. Ther.*, **21** (2013), 170. https://doi.org/10.1016/S1525-0016(16)34775-X
16. M. J. F. Crupi, J. C. Bell , R. Singaravelu, Concise review: Targeting cancer stem cells and their supporting niche using oncolytic viruses, *Stem Cells*, **37** (2019), 716–723. https://doi.org/10.1002/stem.3004

17. S. G. Warner, D. Haddad, J. Au, J. S. Carson, M. P. O'Leary, C. Lewis, et al., Oncolytic herpes simplex virus kills stem-like tumor-initiating colon cancer cells, *Mol. Ther.: Oncol.*, **3** (2016). https://doi.org/10.1038/mto.2016.13

18. R. Rezaei, H. E. G. Ghaleh, M. Farzanehpour, R. Dorostkar, R. Ranjbar, M. Bolandian, et al., Combination therapy with CAR T cells and oncolytic viruses: a new era in cancer immunotherapy, *Cancer Gene Ther.*, **29** (2022), 647–660. https://doi.org/10.1038/s41417-021-00359-9

19. M. D. Johnston, C. M. Edwards, W. F. Bodmer, P. K. Maini, S. J. Chapman, Mathematical modeling of cell population dynamics in the colonic crypt and in colorectal cancer, *Proc. Natl. Acad. Sci.*, **104** (2007), 4008–4013. https://doi.org/10.1073/pnas.0611179104

20. S. A. M. Tonekaboni, A. Dhawan, M. Kohandel, Mathematical modelling of plasticity and phenotype switching in cancer cell populations, *Math. Biosci.*, **283** (2017), 30–37. https://doi.org/10.1016/j.mbs.2016.11.008

21. A. Mahdipour-Shirayeh, K. Kaveh, M. Kohandel, S. Sivaloganathan, Phenotypic heterogeneity in modeling cancer evolution, *PLoS ONE*, **12** (2017), 0187000. https://doi.org/10.1371/journal.pone.0187000

22. D. Wodarz, Viruses as antitumor weapons: defining conditions for tumor remission, *Cancer Res.*, **61** (2001), 3501–3507.

23. M. Agarwal, A. S. Bhadauria, Mathematical modeling and analysis of tumor therapy with oncolytic virus, *Appl. Math.*, **2** (2011), 131–140. https://doi.org/10.4236/am.2011.21015

24. S. Jahedi, L. Wang, J. A. Yorke, J. Watmough, Finding Hopf bifurcation islands and identifying thresholds for success or failure in oncolytic viral therapy, *Math. Biosci.*, **376** (2024), 109275. https://doi.org/10.1016/j.mbs.2024.109275

25. P. van den Driessche, J. Watmough, Reproduction numbers and sub-threshold endemic equilibria for compartmental models of disease transmission, *Math. Biosci.*, **180** (2002), 29–48. https://doi.org/10.1016/S0025-5564(02)00108-6

26. D. Dingli, A. Traulsen, F. Michor, (A) symmetric stem cell replication and cancer, *PLoS Comput. Biol.*, **3** (2007), 83. https://doi.org/10.1371/journal.pcbi.0030053

27. B. Werner, D. Dingli, T. Lenaerts, J. M. Pacheco, A. Traulsen, Dynamics of mutant cells in hierarchical organized tissues, *PLoS Comput. Biol.*, **7** (2011), 1002290. https://doi.org/10.1371/journal.pcbi.1002290

28. T. Shibue, R. A. Weinberg, EMT, CSCs, and drug resistance: The mechanistic link and clinical implications, *Nat. Rev. Clin. Oncol.*, **14** (2017), 611–629. https://doi.org/10.1038/nrclinonc.2017.44

29. L. Vermeulen, E. Morrissey, M. van der Heijden, A. M. Nicholson, A. Sottoriva, S. Buczacki, et al., Defining stem cell dynamics in models of intestinal tumor initiation, *Science*, **342** (2013), 995–998. https://doi.org/10.1126/science.1243148

30. M. van der Heijden, L. Vermeulen, Stem cells in homeostasis and cancer of the gut, *Mol. Cancer*, **18** (2019), 66. https://doi.org/10.1186/s12943-019-0962-x

31. L. Ritsma, S. I. J. Ellenbroek, A. Zomer, H. J. Snippert, F. J. de Sauvage, B. D. Simons, et al., Intestinal crypt homeostasis revealed at single-stem-cell level by in vivo live imaging, *Nature*, **507** (2014), 362–365. https://doi.org/10.1038/nature12972

32. L. Vermeulen, H. J. Snippert, Stem cell dynamics in homeostasis and cancer of the intestine, *Nat. Rev. Cancer*, **14** (2014), 468–480. https://doi.org/10.1038/nrc3744

33. A. Humphries, N. A. Wright, Colonic crypt organization and tumorigenesis, *Nat. Rev. Cancer*, **8** (2008), 415–424. https://doi.org/10.1038/nrc2392

34. H. Wang, N. G. Chen, B. R. Minev, A. A. Szalay, Oncolytic vaccinia virus GLV-1h68 strain shows enhanced replication in human breast cancer stem-like cells in comparison to breast cancer cells, *J. Transl. Med.*, **10** (2012), 167. https://doi.org/10.1186/1479-5876-10-167

35. S. Aref, A. Z. Castleton, K. Bailey, R. Burt, A. Dey, D. Leongamornlert, et al., Type 1 interferon responses underlie tumor-selective replication of oncolytic measles virus, *Mol. Ther.*, **28** (2020), 1043–1055. https://doi.org/10.1016/j.ymthe.2020.01.027

36. N. L. Komarova, D. Wodarz, *Targeted Cancer Treatment in Silico: Small Molecule Inhibitors and Oncolytic Viruses*, Birkhäuser, 2014. https://doi.org/10.1007/978-1-4614-8301-4

37. C. E. Meacham, S. J. Morrison, Tumour heterogeneity and cancer cell plasticity, *Nature*, **501** (2013), 328–337. https://doi.org/10.1038/nature12624

38. A. Marusyk, K. Polyak, Tumor heterogeneity: Causes and consequences, *Biochim. Biophys. Acta-Rev. Cancer*, **1805** (2010), 105–117. https://doi.org/10.1016/j.bbcan.2009.11.002

39. S. Chaurasiya, N. G. Chen, S. G. Warner, Oncolytic virotherapy versus cancer stem cells: A review of approaches and mechanisms, *Cancers*, **10** (2018), 124. https://doi.org/10.3390/cancers10040124

40. S. Yano, H. Tazawa, Y. Hashimoto, Y. Shirakawa, S. Kuroda, M. Nishizaki, et al., A genetically engineered oncolytic adenovirus decoys and lethally traps quiescent cancer stem–like cells in S/G_2/M phases, *Clin. Cancer Res.*, **19** (2013), 6495–6505. https://doi.org/10.1158/1078-0432.CCR-13-0742

41. M. Aghi, T. Visted, R. A. DePinho, E. A. Chiocca, Oncolytic herpes virus with defective ICP6 specifically replicates in quiescent cells with homozygous genetic mutations in p16, *Oncogene*, **27** (2008), 4249–4254. https://doi.org/10.1038/onc.2008.53

42. P. Bach, T. Abel, C. Hoffmann, Z. Gal, G. Braun, I. Voelker, et al., Specific elimination of $CD133^+$ tumor cells with targeted oncolytic measles virus, *Cancer Res.*, **73** (2013), 865–874. https://doi.org/10.1158/0008-5472.CAN-12-2221

43. Q. D. Chu, G. Sun, M. Pope, N. Luraguiz, D. T. Curiel, R. Kim, et al., Virotherapy using a novel chimeric oncolytic adenovirus prolongs survival in a human pancreatic cancer xenograft model, *Surgery*, **152** (2012), 441–448. https://doi.org/10.1016/j.surg.2012.05.040

44. D. Grote, R. Cattaneo, A. K. Fielding, Neutrophils contribute to the measles virus-induced antitumor effect: enhancement by granulocyte macrophage colony-stimulating factor expression, *Cancer Res.*, **63** (2003), 6463–6468.

45. N. L. Komarova, D. Wodarz, ODE models for oncolytic virus dynamics, *J. Theor. Biol.*, **263** (2010), 530–543. https://doi.org/10.1016/j.jtbi.2010.01.009

46. S. Jahedi, *Assessing Oncolytic Viral Therapy and Its Barriers: A Mathematical Approach*, Ph.D thesis, University of New Brunswick, 2022.
47. S. M. Al-Tuwairqi, N. O. Al-Johani, E. A. Simbawa, Modeling dynamics of cancer virotherapy with immune response, *Adv. Differ. Equations*, **2020** (2020), 438. https://doi.org/10.1186/s13662-020-02893-6
48. M. Liu, Z. Ji, V. Jain, V. L. Smith, E. Hocke, A. P. Patel, et al., Spatial transcriptomics reveals segregation of tumor cell states in glioblastoma and marked immunosuppression within the perinecrotic niche, *Acta Neuropathol. Commun.*, **12** (2024), 64. https://doi.org/10.1186/s40478-024-01769-0
49. T. Beneteau, C. Selinger, M. T. Sofonea, S. Alizon, Episome partitioning and symmetric cell divisions: Quantifying the role of random events in the persistence of HPV infections, *PLoS Comput. Biol.*, **17** (2021), 1009352. https://doi.org/10.1371/journal.pcbi.1009352
50. T. D. Zaikos, V. H. Terry, N. T. S. Kettinger, J. Lubow, M. M. Painter, M. C. Virgilio, et al., Hematopoietic stem and progenitor cells are a distinct hiv reservoir that contributes to persistent viremia in suppressed patients, *Cell Rep.*, **25** (2018), 3759–3773. https://doi.org/10.1016/j.celrep.2018.11.104
51. T. Tu, B. Zehnder, J. M. Wettengel, H. Zhang, S. Coulter, V. Ho, et al., Mitosis of hepatitis B virus-infected cells in vitro results in uninfected daughter cells, *JHEP Rep.*, **4** (2022), 100514. https://doi.org/10.1016/j.jhepr.2022.100514
52. A. Goyal, R. M. Ribeiro, A. S. Perelson, The role of infected cell proliferation in the clearance of acute HBV infection in humans, *Viruses*, **9** (2017), 350. https://doi.org/10.3390/v9110350
53. B. Werner, J. G. Scott, A. Sottoriva, A. R. A. Anderson, A. Traulsen, P. M. Altrock, The cancer stem cell fraction in hierarchically organized tumors can be estimated using mathematical modeling and patient-specific treatment trajectories, *Cancer Res.*, **76** (2016), 1705–1713. https://doi.org/10.1158/0008-5472.CAN-15-2069
54. C. D. Meyer, *Matrix Analysis and Applied Linear Algebra*, 2^{nd} edition, Siam, 2023. https://doi.org/10.1137/1.9781611977448

AIMS Press